Applied Catalysis B: Environmental 181 (2016) 47–57

Contents lists available at ScienceDirect

Applied Catalysis B: Environmental

journal homepage: www.elsevier.com/locate/apcatb

Development of cerium promoted copper–magnesium catalysts for biomass valorization: Selective hydrogenolysis of bioglycerol

Baithy Mallesham[a], Putla Sudarsanam[b], Bellala Venkat Shiva Reddy[a], Benjaram M. Reddy[a,*]

[a] Inorganic and Physical Chemistry Division, CSIR—Indian Institute of Chemical Technology, Uppal Road, Hyderabad 500 007, India
[b] Centre for Advanced Materials and Industrial Chemistry (CAMIC), School of Applied Sciences, RMIT University, Melbourne, VIC 3001, Australia

ARTICLE INFO

Article history:
Received 3 May 2015
Received in revised form 22 July 2015
Accepted 24 July 2015
Available online 28 July 2015

Keywords:
Bioglycerol
Hydrogenolysis
1,2-Propanediol
Ce-promoted Cu/Mg catalyst
Characterization studies

ABSTRACT

The selective hydrogenolysis of bioglycerol to 1,2-propanediol was investigated over a series of Ce-promoted Cu/Mg catalysts, namely, Cu/Mg (1/9), Cu/Ce/Mg (1/1/5), Cu/Ce/Mg (1/3/5), and Cu/Ce/Mg (1/5/5) prepared by a coprecipitation method. The physicochemical properties of the synthesized catalysts were analyzed by XRD, Raman, BET, BJH, XPS, NH_3- and CO_2-TPD, and H_2-TPR techniques. The XRD and BET surface area results indicated that addition of Ce to Cu/Mg sample remarkably inhibits the crystal growth of CuO and improves the specific surface area. More number of oxygen vacancy defects were found in the Cu/Ce3/Mg sample, as evidenced from Raman studies. The reducible nature of the Cu/Mg sample was significantly enhanced after the Ce-incorporation. The NH_3- and CO_2-TPD results show that the acid–base properties of the Ce-promoted Cu/Mg samples are highly dependent on the Ce-loading. Among the synthesized samples, the Cu/Ce3/Mg sample exhibited higher concentration and superior strength of acidic sites. The achieved activity order of various catalysts for glycerol hydrogenolysis is Cu/Mg < Cu/Ce1/Mg < Cu/Ce3/Mg < Cu/Ce5/Mg. The high surface area, higher concentration of acid sites, abundant oxygen vacancies, and remarkable reducibility are found to be the key factors for the observed superior performance of the Cu/Ce3/Mg catalyst. Notably, the Cu/Ce3/Mg catalyst could be used multiple times for glycerol hydrogenolysis without considerable loss of activity.

1. Introduction

We are presently facing significant economic and environmental challenges due to ever-increasing oil prices and negative impacts of fossil fuels. The utilization of alternative viable renewable energy sources, such as biomass, solar, wind, geothermal, and tidal powers is essential to decrease our dependence on the fossil fuels [1–3]. In particular, biomass represents an alternative viable energy source to fossil fuels due to its high abundance, remarkable sustainability, and CO_2-neutral emissions [4–6]. The production of fuels and chemicals from biomass-derived platform molecules is one of the best solutions to reduce our dependence on fossil resources and to solve the environmental problems. In this context, the most attractive and potential approach is to convert bioglycerol into value-added biofuels and chemicals [7]. Glycerol, a byproduct produced (~10 wt.%) from biodiesel synthesis process, is considered as one of the top platform chemicals estimated by the US Department of Energy [7,8].

A number of value-added biofuels and chemicals can be produced from bioglycerol, including 1,2 and 1,3-propanediols, cyclic acetals/ketals, glycerol carbonates, glycerol esters, glycerol ethers, glyceric acid, and acrolein/acrylic acid as well as many other specialty chemicals [9–16]. Among various utilization routes of glycerol, the selective hydrogenolysis of glycerol to 1,2-propanediol (1,2-PDO) is of paramount research interest to the scientific community. The 1,2-PDO is a vital desirable chemical that can be used in a wide variety of industrial applications, such as pharmaceuticals, antifreeze additives, cosmetics, polymers, tobacco industries, etc. [17–19]. 1,2-PDO is usually produced by a petrochemical approach through the hydration of hazardous propylene oxide, which is an expensive and environmentally unfriendly method [7]. On the other hand, the synthesis of 1,2-PDO from the hydrogenolysis of bioglycerol using catalytic materials is obviously a highly sustainable and economical route [9].

Two types of heterogeneous catalytic systems have been mostly studied for the glycerol hydrogenolysis: noble metal-based catalysts (e.g., Ru-, Au-, Pt-, Pd-, and Rh-based catalysts) [20–24] and

* Corresponding author. Fax: +91 40 2716 0921.
E-mail addresses: bmreddy@iict.res.in, mreddyb@yahoo.com (B.M. Reddy).

http://dx.doi.org/10.1016/j.apcatb.2015.07.037
0926-3373/

non-noble metal-based catalysts (e.g., Cu- and Ni-based catalysts) [25–28]. High cost, low thermal stability, and much low efficiency toward the 1,2-PDO selectivity are the main disadvantages of the noble metal based catalysts [21,22]. On the other hand, the use of Ni-based catalysts favor the C–C bond cleavage, thus resulting in low 1,2-PDO selectivity [29]. Above all, the Cu-based catalysts show a better performance for the hydrogenation–dehydrogenation of C–O bonds and low efficiency toward C–C bond cleavage [27,30]. The Cu-based catalysts can be therefore considered as the promising materials for both achieving high glycerol conversion and superior selectivity of the 1,2-PDO [31–33]. Especially, the Cu/Mg catalytic systems have been used in glycerol hydrogenolysis due to their remarkable ability in obtaining high selectivity of 1,2-propanediol [32,33]. However, there are several concerns about the deactivation of the Cu/Mg catalysts in the glycerol hydrogenolysis [32]. Therefore, there is a great deal of research interest in enhancing the efficiency of the Cu/Mg catalysts for the hydrogenolysis of glycerol.

The use of cerium (Ce) as an additive/promoter for the hydrogenation catalysts has attracted much attention because it shows an excellent promoting effect in the hydrogenolysis reactions [34–36]. Huang et al. reported that the addition of rare earth metals including Ce to Cu/SiO_2 catalysts significantly enhances its catalytic performance toward selective hydrogenolysis of glycerol to 1,2-PDO, which could promote the stability and prevent the sintering and leaching of the active Cu species [28]. The enhancement in the acid–base properties and improved synergetic effect between the Ce and active metal phase are the key factors for better performance of the Ce-promoted catalysts in the hydrogenolysis reactions. Motivated by the above considerations, in this work we have prepared a series of Ce-promoted Cu/Mg catalysts by a coprecipitation method. The catalytic efficiency of the Ce-promoted Cu/Mg materials was studied for the hydrogenolysis of glycerol. A wide variety of spectroscopic and non-spectroscopic techniques, such as X-ray diffraction (XRD), BET surface area, Barrett–Joyner–Halenda (BJH) pore size distribution, X-ray photoelectron spectroscopy (XPS), Raman spectroscopy, H_2-temperature programmed reduction (H_2-TPR) and NH_3- and CO_2-temperature programmed desorption (NH_3- and CO_2-TPD) measurements were employed to examine the structural, redox, and acid–base properties of the Ce-promoted Cu/Mg catalysts. The effect of reaction time, catalyst wt.%, glycerol concentration, H_2-pressure, water quantity, and the temperature on glycerol hydrogenolysis is investigated in detail. Much attention has been paid to correlate the catalytic activity results with the characterization studies.

2. Experimental

2.1. Catalyst preparation

The Ce-promoted Cu/Mg catalysts were prepared by a coprecipitation method from dilute aqueous solutions. Coprecipitation of the metal ions was carried out by dissolving the requisite amounts of $Cu(NO_3)_2{\cdot}2.5H_2O$ (Aldrich, AR grade), $Ce(NO_3)_3{\cdot}6H_2O$ (Aldrich, AR grade), and $Mg(NO_3)_2{\cdot}6H_2O$ (Aldrich, AR grade) precursors in 500 mL of double distilled water under vigorous stirring conditions with a mechanical stirrer. Then, the precipitating agent (0.5 M NaOH) was drop wise added to the above solution until pH of the solution reaches ~10 at 343 K temperature. The obtained freshly precipitated slurry was filtered off, washed with 1000 mL hot deionized water followed by normal deionized water until the pH of the filtrate solution reaches ~7 and then oven-dried at 383 K for 12 h. Finally, the sample was calcined at 773 K for 5 h with a heating rate of 5 K min^{-1} under atmospheric air. For comparison, an un-promoted Cu/Mg and pristine CeO_2 were also synthesized using the same procedure. For convenience, the prepared samples, namely, CeO_2, Cu/Mg (atomic ratio = 1/9), Cu/Ce/Mg (1/1/5), Cu/Ce/Mg (1/3/5) and Cu/Ce/Mg (1/5/5) are designated with CeO_2, Cu/Mg, Cu/Ce1/Mg, Cu/Ce3/Mg and Cu/Ce5/Mg, respectively.

2.2. Catalyst characterization

The powder X-ray diffraction (XRD) profiles of the samples were obtained on a Rigaku Multiflex diffractometer equipped with a nickel-filtered Cu Kα (0.15418 nm) radiation source and a Scintillation counter detector. The XRD data were collected from 2θ values of 2–80° by scanning at 0.01° steps with a counting time of 1 s at every step.

Raman spectra were recorded at room temperature on a Horiba Jobin-Yvon HR800 Raman spectrometer equipped with a liquid-nitrogen cooled charge coupled device (CCD) detector and a confocal microscope. The line at 632 nm Ar^+ ion (Spectra Physics) laser was used as excitation source. The laser was focused on the sample under a microscope with the diameter of the analyzed spot being ~1 μm. The acquisition time was adjusted according to the intensity of the Raman scattering. The wavenumber values reported are accurate to within 1 cm^{-1}.

Specific surface areas of the samples were determined by BET analysis of the N_2 adsorption–desorption isotherms at liquid N_2 temperature (77 K). A Micromeritics ASAP 2020 instrument was employed for this purpose. Prior to the experiment, samples were degassed at 423 K for 3 h to remove any adsorbed surface residual moisture. The specific surface areas were calculated from adsorption data in the relative pressure (P/P_o) range = 0.04–0.25.

The XPS analysis was carried out using a Shimadzu (ESCA 3400) spectrometer with Mg Kα radiation source (1253.6 eV). The analysis was done at room temperature and the samples were continued in a rigorous vacuum typically in the order of less than 10^{-8} Pa to avoid noise in the spectra from contaminates. All binding energies were measured within a precision of ±0.2 eV. The binding energies were charge corrected by setting the binding energy (BE) of the adventitious carbon (C 1s) peak at 284.6 eV.

The H_2-TPR experiments were performed using a tubular quartz reactor coupled with a TCD of gas chromatograph (Shimadzu). A 30 mg of fresh sample was loaded in an isothermal zone of the reactor and heated at a rate of 10 K min^{-1} from room temperature to 573 K in 30 mL min^{-1} He gas, which facilitates desorption of the physically adsorbed water. After the reactor was cooled to room temperature, He was switched to 10% H_2 in Ar with a rate of 20 mL min^{-1} and the temperature was linearly raised to 1073 K at a continuous heating ramp of 5 K min^{-1}, keeping all other parameters constant. The hydrogen consumption during the reduction was calculated by passing the effluent gas through a molecular sieve trap to remove the produced water and was analyzed by gas chromatograph using the TCD.

The NH_3- and CO_2-TPD measurements were performed on a Micromeritics AutoChem 2910 instrument. A thermal conductivity detector was used for continuous monitoring of the desorbed gas. Prior to TPD measurements, samples were pre-treated at 573 K for 1 h and then saturated with 4.95% of NH_3 or 9.72% of CO_2 (balance He) with a flow rate of 20 mL min^{-1} for 1 h, and subsequently flushed with He to remove the physisorbed gas. The chemisorbed amount of NH_3 and/or CO_2 was measured in flowing He gas with a flow rate of 20 mL min^{-1} from 373 to 1073 K at a heating rate of 10 K min^{-1}.

2.3. Catalytic activity measurement

The selective hydrogenolysis of glycerol was performed in a 200 mL stainless steel autoclave equipped with an electronic temperature controller and a mechanical stirrer. Unless specifically

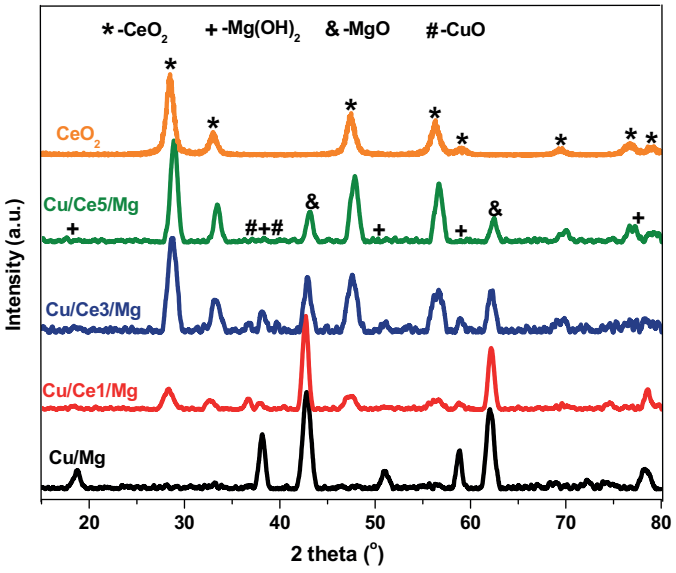

Fig. 1. Powder X-ray diffraction patterns of Cu/Mg, Cu/Ce1/Mg, Cu/Ce3/Mg, Cu/Ce5/Mg, and bare CeO_2 sample.

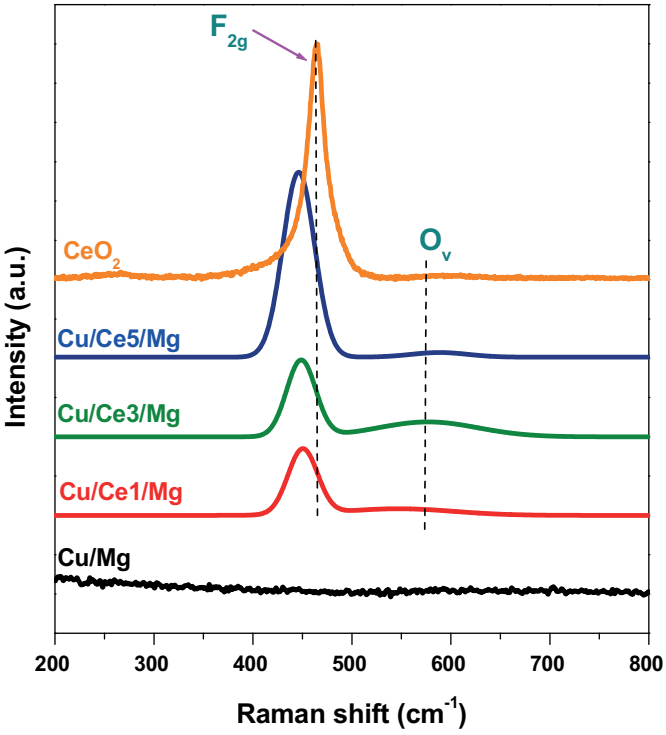

Fig. 2. Visible Raman spectra of Cu/Mg, Cu/Ce1/Mg, Cu/Ce3/Mg, and Cu/Ce5/Mg catalysts.

stated, all the synthesized catalysts were reduced at 573 K with a hydrogen flow rate of 20 mL min^{-1} for 3 h. After the reduction of the catalyst, the reactor was cooled to room temperature and then, the reduced catalyst was immediately added to the aqueous glycerol solution exclusive of further delay. The standard reaction was carried out under the following conditions: 473 K of reaction temperature, 60 bar of H_2 pressure, 50 g of 20 wt.% aqueous glycerol solution, 1 g of reduced catalyst, stirring speed of 300 rpm, and 10 h of reaction time. After completion of the reaction, the autoclave was cooled to room temperature and the pressure was released carefully. Then the catalyst was separated from the reaction mixture by centrifugation. The liquid products were analyzed by Nucon 5785 gas chromatograph equipped with a PEG-20 M capillary column and a flame ionization detector (FID). The products were identified using authentic samples and also identified by GC–MS with QP 5050A (Shimadzu Instruments, Japan). The conversion of glycerol and the selectivity of 1,2-PDO were estimated as per the established procedures [16].

3. Results and discussion

3.1. Catalyst characterization

The XRD patterns of the un-promoted and Ce-promoted Cu/Mg catalysts, with the pure CeO_2 are shown in Fig. 1. The detailed analysis of the XRD patterns reveal the existence of different phases related to CuO, MgO, and CeO_2 in the prepared samples. It is interesting to mention here that the Cu/Ce1/Mg and Cu/Ce3/Mg samples show various XRD peaks corresponding to CuO phases, whereas no XRD peaks are observed for the metallic Cu phase [31–33]. On the other hand, no XRD peaks corresponding to both CuO and Cu phases were found in the case of Cu/Mg and Cu/Ce5/Mg catalysts. All the Ce-promoted Cu/Mg samples show various characteristic peaks at 2 theta values of 28.65, 33.03, 47.46, 56.31, 59.06, 69.41, 76.66, and 79.03° (JCPDS 34-0394), indicating the fluorite cubic structured CeO_2. The CeO_2 diffraction peaks of Ce-promoted Cu/Mg samples are shifted to higher angle side compared with that of the pure CeO_2. This unusual observation could be due to the interaction between the CeO_2 and Cu/Mg sample. In addition, the un-promoted Cu/Mg and Ce-promoted Cu/Mg samples exhibit two major XRD peaks at around 42.8 and 62.1°, which indicate the MgO phase. As well, the peaks observed at 19, 38, 51 and 59° are assigned to $Mg(OH)_2$ species of the samples [32,37]. It is interesting to note that the intensity of CuO peaks is low in comparison with the peaks of CeO_2 and MgO. This observation might be due to poor crystalline nature of the CuO and/or formation of mixed oxides with Ce and/or Mg.

Using the most intense line CeO_2 (1 1 1) of the XRD patterns, the calculation of CeO_2 lattice parameters '*a*' of the samples was carried out. The obtained values are summarized in Table 1. Decreased lattice parameters were found for the Cu/Ce1/Mg, Cu/Ce3/Mg, and Cu/Ce5/Mg samples compared with the pristine CeO_2. The CuO average crystallite size of various samples was calculated using the Debye–Scherrer equation (by using peak at $2\theta = 36$). The obtained results are presented in Table 1. The average CuO crystallite sizes of the Cu/Ce1/Mg and Cu/Ce3/Mg samples were found to be 12.8 and 10.1 nm, respectively. It is clear from the crystallite size measurements that the Cu/Ce3/Mg sample has smaller CuO crystallite size, which might be due to well-dispersion of CuO species on the catalyst surface. Wang and Liu et al. reported that smaller sized CuO particles show better catalytic efficiency for the hydrogenolysis of glycerol with high selectivity of 1,2-PDO [34]. It is therefore expected that the Cu/Ce3/Mg catalyst shows better performance for the hydrogenolysis of glycerol compared with that of other catalysts, which is discussed in the later paragraphs [31,38].

Raman spectra of the un-promoted Cu/Mg, Ce-promoted Cu/Mg and pure CeO_2 samples are shown in Fig. 2. All the samples exhibited a major Raman peak at ~450 cm^{-1}, which indicates the triply degenerate F_{2g} mode of oxygen anions around the cerium cations [39,40]. This result reveals the formation of cubic structured CeO_2 in the synthesized samples, in line with the XRD results (Fig. 1). As can be noted from Fig. 2, the F_{2g} band is shifted to lower wavenumbers for all the Cu/Mg based catalysts compared with the pure ceria. The variation in the F_{2g} position could be attributed to several factors, including phonon confinement, defects, strain, and variations in the particle size [39–41]. In addition, the Ce-promoted Cu/Mg samples showed a weak peak at 585 cm^{-1}, which indicates the presence

Table 1
BET surface area (S_{BET}), pore volume (V_p), CuO crystallite size (D_{CuO}), lattice parameter (A), intensity ratio of the O_v band to the F_{2g} band (I_{Ov}/I_{F2g}), acidic sites (AS), and basic sites (BS) of catalysts.

Sample	Composition	S_{BET} ($m^2\ g^{-1}$)	V_p ($cm^3\ g^{-1}$)	D_{CuO} (nm)[a]	A (nm)[a]	I_{Ov}/I_{F2g}[b]	AS (μmol/g)[c]	BS (μmol/g)[d]
Cu/Mg	1:9	119	0.201	n.d.	n.d.	n.d.	73	164
Cu/Ce1/Mg	1:1:5	170	0.526	12.8	5.38	0.379	165	122
Cu/Ce3/Mg	1:3:5	209	0.569	10.1	5.39	0.941	521	108
Cu/Ce5/Mg	1:5:5	194	0.548	n.d.	5.36	0.102	440	110

n.d.: not determined.
[a] Estimated from XRD studies.
[b] Obtained from Raman analysis.
[c] Determined from NH_3-TPD.
[d] Determined from CO_2-TPD studies.

of oxygen vacancy defects (O_v) in the ceria lattice. The intensity of this peak is quite high for the Cu/Ce3/Mg sample compared with that of all other samples. The estimated I_{Ov}/I_{F2g} values were found to be ~0.378, 0.941, and 0.102 for the Cu/Ce1/Mg, Cu/Ce3/Mg, and Cu/Ce5/Mg catalysts, respectively. It was obvious that the Cu/Ce3/Mg sample shows more number of oxygen vacancy defects compared with the Cu/Ce1/Mg and Cu/Ce5/Mg samples. Oxygen vacancy defects play a favorable role in the glycerol hydrogenolysis, which is discussed in the activity part.

The obtained N_2 adsorption–desorption isotherms reveal that all the Ce-promoted Cu–Mg samples exhibit Type IV isotherms with typical H1 hysteresis loops, which are characteristic of mesoporous materials (Fig. S1 of the Supplementary material) [6]. The appearance of hysteresis loops indicate the enhanced pore size as well as pore connectivity of the Ce-promoted Cu/Mg materials with homogeneous distribution. On the other hand, the un-promoted Cu/Mg sample showed a typical H_2-type hysteresis loop, which is possibly due to the formation of spherical pores along with the cylindrical pores present in the material [42]. The obtained BET surface area and pore volume of the samples are summarized in Table 1. Both BET surface area and pore volume are increased after the Ce addition. The BET surface area of the Cu/Mg, Cu/Ce1/Mg, Cu/Ce3/Mg and Cu/Ce5/Mg samples are found to be approximately 119, 170, 209 and 194 m^2/g, respectively (Table 1). The obtained pore volumes of the Cu/Mg, Cu/Ce1/Mg, Cu/Ce3/Mg, and Cu/Ce5/Mg catalysts are ~0.201, 0.526, 0.569 and 0.548 $cm^3\ g^{-1}$, respectively (Table 1). The pore size distribution curves of the catalysts are shown in Fig. 3. All the samples exhibited a bimodal pore size distribution. Among the Ce-promoted Cu/Mg catalysts, the Cu/Ce3/Mg sample shows the highest specific surface area and pore volume compared with that of other samples.

The XPS analysis was undertaken to know the oxidation states of the elements present in the synthesized catalysts. Fig. 4 shows the Cu 2p core level XPS spectra of the catalysts. The presence of Cu $2p_{3/2}$ lines at approximately 932.4, 932.6, and 933.8 eV indicates Cu^+, Cu^0, and Cu^{2+}, respectively [26,32,43]. As can be noted from Fig. 4, the peak maxima of Cu $2p_{3/2}$ of the Cu/Mg, Cu/Ce1/Mg, Cu/Ce3/Mg and Cu/Ce5/Mg samples were observed at ~933.7, 934.1, 934.2, and 932.7 eV along with a satellite peak between ~941 and 944 eV, respectively. These results indicate that all the catalysts are dominated by CuO phase with a small amount of Cu_2O or metallic Cu [26,43]. Interestingly, the Cu 2p core level features in the Cu/Ce3/Mg sample are shifted to high binding energy compared with other samples, which indicate the improvement of

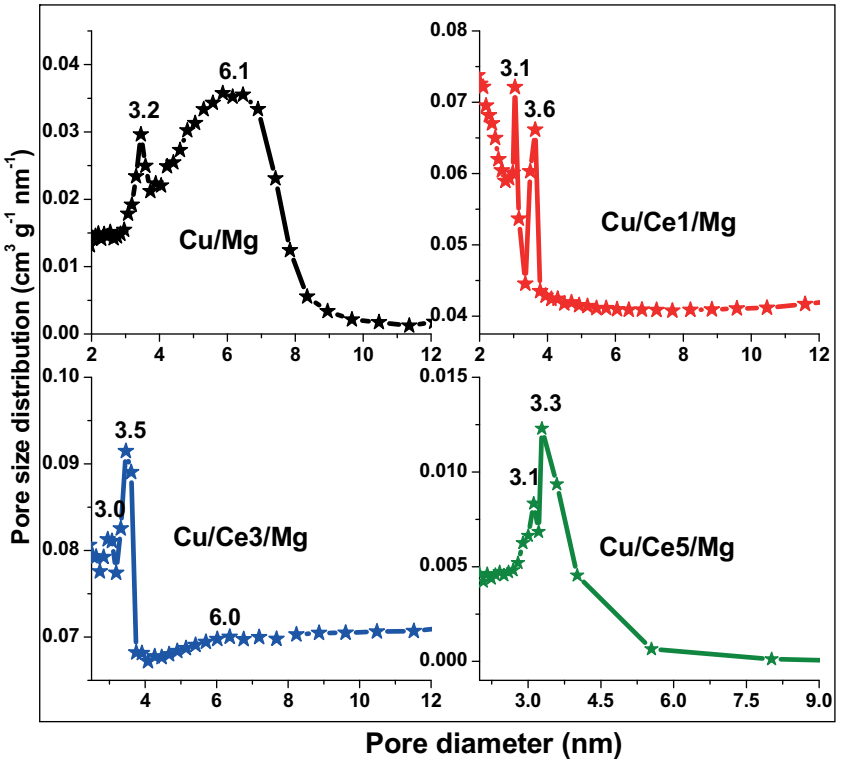

Fig. 3. Pore size distribution profiles of Cu/Mg, Cu/Ce1/Mg, Cu/Ce3/Mg, and Cu/Ce5/Mg catalysts.

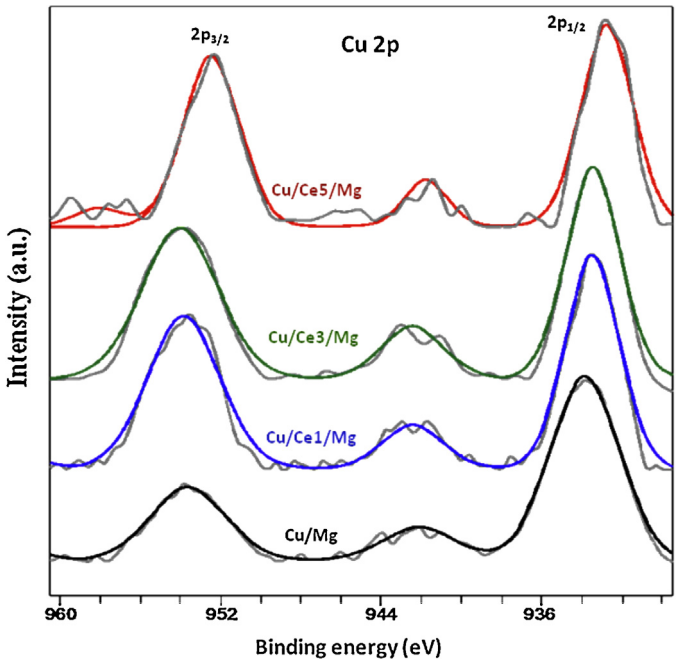

Fig. 4. Cu 2p XP spectra of Cu/Mg, Cu/Ce1/Mg, Cu/Ce3/Mg, and Cu/Ce5/Mg samples.

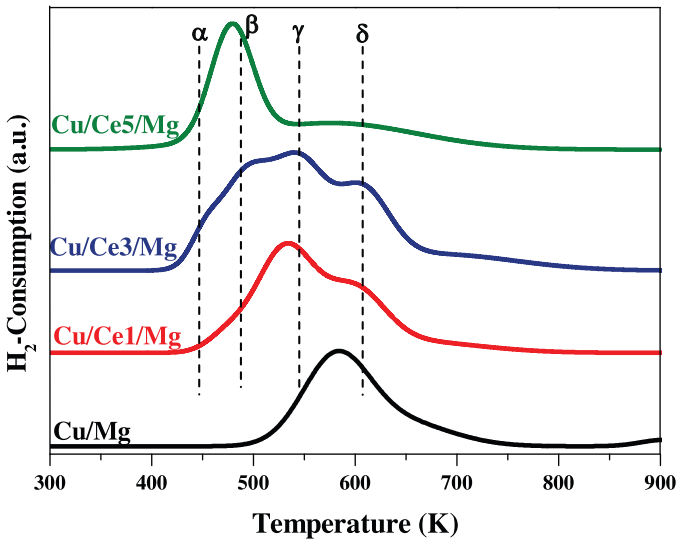

Fig. 5. H_2-TPR profiles of Cu/Mg, Cu/Ce1/Mg, Cu/Ce3/Mg, and Cu/Ce5/Mg samples.

charge transfer from the copper metal ions to the CeO_2 and/or MgO species [44]. This observation is due to either the strong interaction between the copper oxide species and CeO_2 and/or MgO or a well dispersion of copper oxide particles [45–47].

The obtained Ce 3d XPS spectra are complex due to the hybridization of Ce 4f with ligand orbitals and fractional occupancy of the valence 4f orbital (Fig. S2 of the Supplementary material). As per the literature, the peaks are labeled with '*u*', due to $3d_{3/2}$ spin-orbit states and those labeled with '*v*' reveal $3d_{5/2}$states [40,41]. The v^{I} and u^{I} peaks confirm the Ce in 3+ oxidation state, whereas the *v*, v^{II}, v^{III}, *u*, u^{II}, and u^{III} peaks signify the Ce in 4+ oxidation state. The peaks at ~917.2 and 898.6 eV represent u^{III} and v^{III}, which are the main characteristic lines for Ce $3d_{3/2}$ and Ce $3d_{5/2}$ states, respectively. A close observation of the XPS spectra reveals that the u^{III} peak area of Cu/Ce3/Mg sample is quite lower compared to other samples. This observation indicates that the Cu/Ce3/Mg sample contains more number of Ce^{3+} ions [39–41]. The formation of oxygen vacancies in the synthesized samples is the key reason for the reduction of Ce^{4+} ions to Ce^{3+} [48,49]. It is a well-known fact that the concentration of Ce^{3+} ions is proportional to that of oxygen vacancy defect sites. It is therefore confirmed that the presence of more number of Ce^{3+} ions in the Cu/Ce3/Mg sample is due to abundant oxygen vacancies (Fig. 2). The obtained Mg 2p spectra indicate that all the samples contain the Mg^{2+} species (Fig. S3a of the Supplementary material) [50]. On the other hand, the O 1s spectra are composed of more than one type of oxygen ions (Fig. S3b of the Supplementary material). Hence, the achieved O 1s spectra can be fitted into two peaks. The peak at lower binding energy side reveals the lattice oxygen, whereas the peak at higher binding energy side indicates the surface carbonates and hydroxyl species [48,49].

Fig. 5 shows the H_2-TPR profiles of the Ce-promoted Cu/Mg and the un-promoted Cu/Mg samples. A number of peaks can be observed in the temperature range of 420–675 K [51]. To get more insight into the TPR results, the peak assignment has been made in Fig. 5. The Cu/Mg sample shows a major peak at around 570 K, indicating the reduction of the copper oxide species. Interestingly, this peak was shifted to lower temperature after the addition of Ce to the Cu/Mg sample. This result indicates that the addition of Ce to the Cu/Mg material exhibits a promoting effect toward low temperature reduction of the CuO species. As shown in Fig. 5, the assigned peaks β and γ are attributed to the reduction of the dispersed CuO species and the bulk reduction of CuO species, respectively [52,53]. Among all the Ce-promoted samples, only the Cu/Ce3/Mg sample showed a low temperature peak (α peak), which is attributed to the reduction of highly dispersed CuO species strongly interacting with the CeO_2 and MgO. The peak appeared at high temperature region (δ peak) can be ascribed to Cu^{2+}/Cu^{+} species having interactions with either CeO_2 or MgO [32]. It is therefore confirmed that the addition of Ce to the Cu/Mg catalyst makes easy reduction of the CuO species [46]. The specific changes in the peaks can be explained based on the interactions between the copper oxide species and CeO_2 and/or MgO species. The small peak at ~750 K can be assigned to the reduction of bulk ceria from CeO_2 to Ce_2O_3. As per the literature, the classification of each TPR peaks in copper–ceria samples are difficult because of the facile reduction and structural similarities of these materials. The facile reduction of the sample is a vital factor for the hydrogenolysis of the glycerol, which is clearly discussed in the activity part. Nonetheless, it is difficult to exactly determine the sequential reduction peaks of copper oxide to metallic copper ($Cu^{2+} \rightarrow Cu^{+} \rightarrow Cu^{0}$) [37,51,54].

The acidic properties of the un-promoted Cu/Mg and Ce-promoted Cu/Mg catalysts are studied by NH_3-TPD analysis. The achieved results are presented in Fig. 6 and Table 1. A prominent peak was found in the range of 580–680 K, which indicates the presence of medium acidic sites in the samples. The intensity of this peak is quite high for the Cu/Ce3/Mg sample. Another interesting observation is that the Cu/Ce3/Mg sample has a weak peak at ~710 K. This peak reveals the presence of strong acidic sites. The calculated amount of acidic sites was found to be ~73, 165, 521 and 440 μmol/g for the Cu/Mg, Cu/Ce1/Mg, Cu/Ce3/Mg, and Cu/Ce5/Mg samples, respectively.

The basic properties of the un-promoted Cu/Mg and Ce-promoted Cu/Mg samples are investigated by CO_2-TPD technique (Fig. 7). The estimated total number of basic sites is represented in Table 1. A major peak at around 680 K was found for all the catalysts, which indicates the existence of the medium basic sites. A broad peak at ~710 K was noticed for the Ce-promoted Cu/Mg catalysts. This peak obviously reveals the formation of strong basic sites in the Ce-promoted Cu/Mg catalysts. It is therefore proved that the addition of Ce to the Cu/Mg sample results in the generation of the strong basic sites. It is interesting to note here that the Cu/Ce3/Mg sample has a higher intensity peak of the strong basic

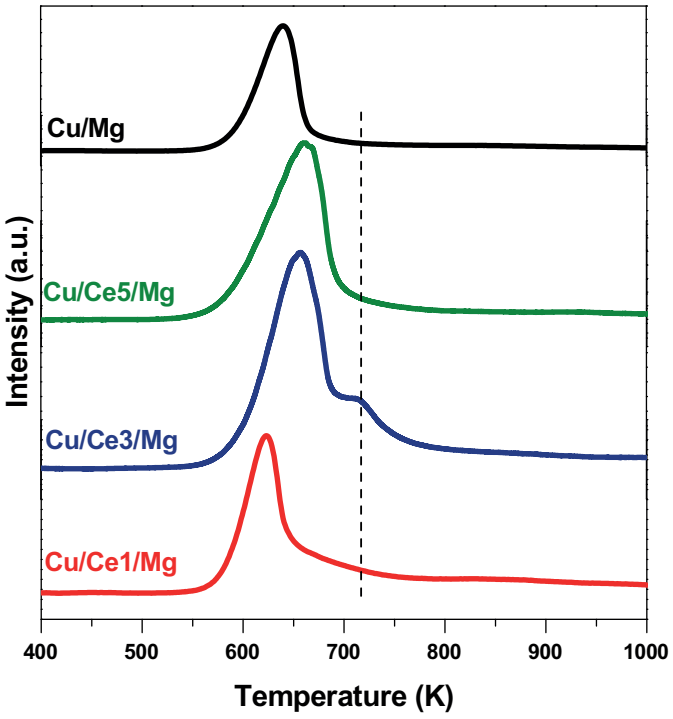

Fig. 6. NH_3-TPD profiles of Cu/Mg, Cu/Ce1/Mg, Cu/Ce3/Mg, and Cu/Ce5/Mg catalysts.

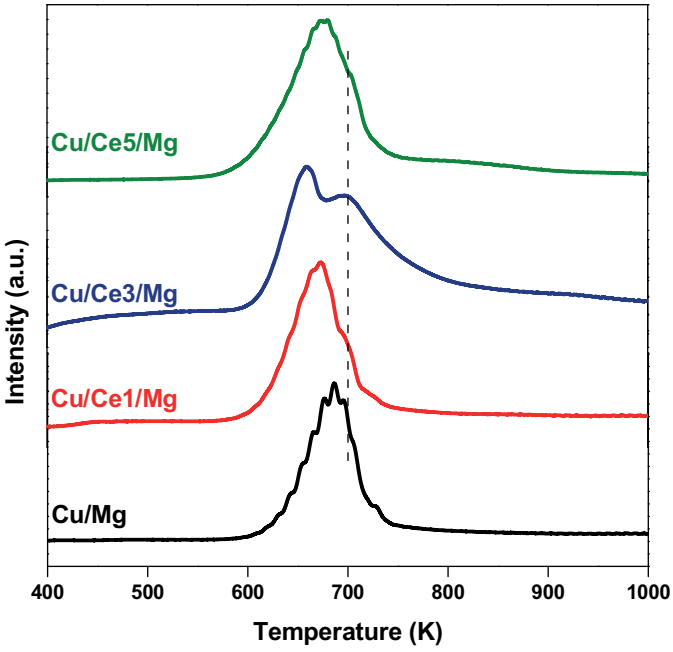

Fig. 7. CO_2-TPD profiles of Cu/Mg, Cu/Ce1/Mg, Cu/Ce3/Mg and Cu/Ce5/Mg catalysts.

sites compared with the Cu/Ce1/Mg and Cu/Ce5/Mg samples. The estimated basic sites are ~164, 122, 108, and 110 μmol/g for the Cu/Mg, Cu/Ce1/Mg, Cu/Ce3/Mg, and Cu/Ce5/Mg samples, respectively. It was obvious from Figs. 6 and 7 that the Ce-promoted Cu/Mg samples show more number of acid sites and less number of basic sites compared with the un-promoted Cu/Mg catalyst.

3.2. Glycerol hydrogenolysis studies

The hydrogenolysis of glycerol using the Ce-promoted and un-promoted Cu/Mg catalysts was performed and the obtained results

Table 2
Selective hydrogenolysis of gycerol over Cu/Mg, Cu/Ce1/Mg, Cu/Ce3/Mg, and Cu/Ce5/Mg catalysts. 1,2-PDO: 1,2-propanediol and EG: ethylene glycol.

Catalysts	Glycerol conversion (%)	Product		
		Selectivity (%)	1,2-PDO EG	Others
Cu/Mg	30.9	90.3	4.2	5.5
Cu/Ce1/Mg	42.6	95.1	1.8	3.1
Cu/Ce3/Mg	56.4	97.4	1.4	1.2
Cu/Ce5/Mg	47.8	93.8	2.0	4.2

Reaction conditions: 50 g of 20 wt.% aqueous glycerol solution, 473 K of temperature, 60 bar of H_2 pressure, 1 g of reduced catalyst, 300 rpm of stirring speed, and 10 h of reaction time.

are presented in Table 2. The catalytic experiments were conducted at 473 K temperature, 60 bar of H_2 pressure, 50 g of 20 wt.% aqueous glycerol solution, 1 g of reduced catalyst, 300 rpm of stirring speed, and 10 h of reaction time. The obtained glycerol conversions and the selectivity of 1,2-PDO were ~30.9 and 90.2% for the un-promoted Cu/Mg sample, respectively. It was found that the addition of Ce to the Cu/Mg sample markedly enhances its performance toward hydrogenolysis of glycerol. The achieved glycerol conversions were ~42.6, 56.4 and 47.8% for the Cu/Ce1/Mg, Cu/Ce3/Mg, and Cu/Ce5/Mg catalysts, respectively. As well, the 1,2-PDO selectivity was found to be ~95.1, 97.4 and 93.8% for the Cu/Ce1/Mg, Cu/Ce3/Mg, and Cu/Ce5/Mg catalysts, respectively. It is therefore clear from Table 2 that the higher glycerol conversion with superior selectivity of 1,2-PDO was found for the Ce-promoted Cu/Mg catalysts. The high catalytic activity of Ce-promoted Cu/Mg catalysts could be attributed to several improved physicochemical properties, such as higher surface area, abundant oxygen vacancies, higher concentration and superior strength of acid sites and remarkable reducibility properties. The BET surface area of the Cu/Mg sample was considerably improved after the Ce-addition (Table 1). In the glycerol hydrogenolysis, the initial step is adsorption of glycerol on the catalyst surface (Scheme 1). It is well-known that the catalyst having higher surface area provides more number of active sites. Hence, more number of glycerol molecules can be adsorbed on the surface of Ce-promoted Cu/Mg catalysts as they exhibit higher surface area compared with that of the un-promoted Cu/Mg catalyst [55,56]. Raman analysis revealed the presence of abundant oxygen vacancies in the Ce-promoted Cu/Mg samples (Fig. 2 and Table 1). These oxygen vacancy defects could play a key role in the glycerol dehydration step to yield the acetol followed by the hydrogenation of acetol on the metallic copper sites to give the 1,2-PDO product [57]. The NH_3-TPD results demonstrated that the addition of Ce to Cu/Mg sample results in higher amount and superior strength of acid sites (Fig. 6). These acid sites play a key role in the dehydration of glycerol to give the acetol and consequently to yield 1,2-PDO. It can be observed from the H_2-TPR profile that the reducible nature of the copper oxide species of Cu/Mg sample was notably enhanced after the Ce-incorporation (Fig. 5). These reduced copper metal species are very important for the hydrogenation of acetol intermediate to obtain the desired 1,2-PDO (Scheme 1). Therefore, all these improved physicochemical properties of the Ce-promoted Cu/Mg samples are found to be play a favorable role for the hydrogenolysis of glycerol to 1,2-PDO.

Among the Ce-promoted Cu/Mg catalysts, the Cu/Ce3/Mg sample showed higher efficiency in the glycerol hydrogenolysis (Table 2). The investigated characterization studies revealed that more favorable properties like, higher BET surface area, large amount and superior strength of acid sites, and abundant oxygen vacancy defect sites were found for the Cu/Ce3/Mg catalyst, hence higher catalytic efficiency toward the glycerol hydrogenolysis.

The selective hydrogenolysis of glycerol to propandiols usually follows the addition of H_2 and the subsequent removal of oxygen in the form of H_2O. For this reaction, a variety of reac-

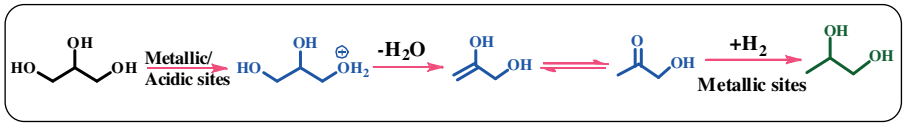

Scheme 1. Reaction pathway leading to synthesis of 1,2-propanediol from hydrogenolysis of glycerol.

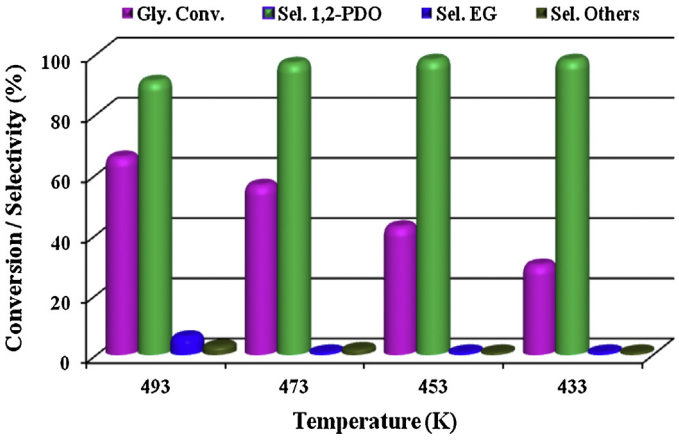

Fig. 8. Effect of temperature on the glycerol conversion and the selectivity of 1,2-PDO over the Cu/Ce3/Mg catalyst. Reaction conditions: 50 g of 20 wt.% aq. glycerol solution, 1 g of reduced catalyst, 60 bar of H_2 pressure and 300 rpm of stirring speed with 10 h of reaction time.

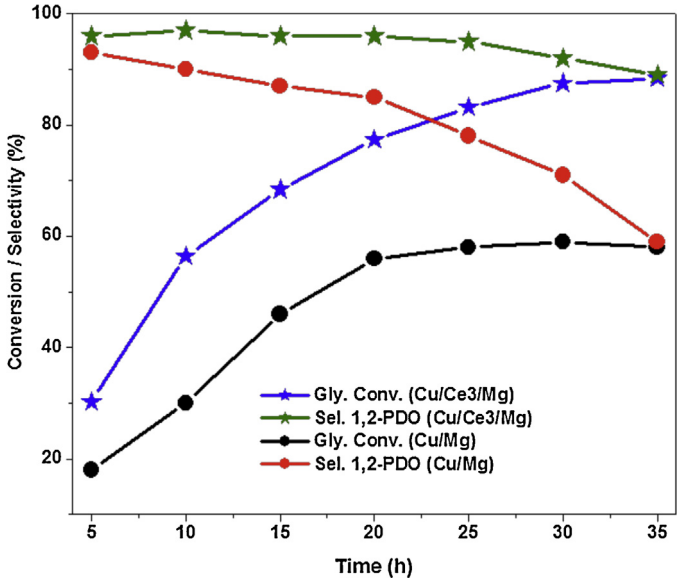

Fig. 9. Effect of reaction time on the glycerol conversion and the selectivity of 1,2-PDO over the Cu/Ce3/Mg catalyst. Reaction conditions: 50 g of 20 wt.% aqueous glycerol solution, 1 g of reduced catalyst, 60 bar of H_2 pressure, and 300 rpm of stirring speed with 473 K of reaction temperature.

tion mechanisms have been reported in the literature. Montassier et al. proposed a mechanism for the formation of 1,2-PDO in glycerol hydrogenolysis reaction via the formation of glyceraldehyde intermediate over the Ru- and Cu-based catalysts [21,55,58–60]. Conversely, the formation of 1,2-PDO from glycerol can also proceed through an acid-catalyzed dehydration of glycerol to acetol intermediate [22,37,61]. More interestingly, the Cu^+ and/or Cu may also play an important role in promoting the dehydration of glycerol to produce acetol [55,59,65]. Based on the above literature reports, we have proposed a plausible mechanism via dehydration–hydrogenation for the glycerol hydrogenolysis over the Cu/Ce3/Mg catalyst (Scheme 1). In this pathway, the glycerol hydrogenolysis involves the acetol formation from the dehydration of glycerol over the acidic and/or metallic sites (Scheme 1). The acidic and/or metallic Cu sites react with primary —OH group of the glycerol to produce dehydration product, which eventually rearranged to acetol. Afterwards, a consecutive reaction by the hydrogenation of acetol with H_2 occurs to give 1,2-PDO product.

Fig. 8 shows the effect of reaction temperature on the hydrogenolysis of glycerol from 433 to 493 K over the Cu/Ce3/Mg sample. The glycerol conversion was increased from 19 to 65% with increased reaction temperature from 433 to 493 K, respectively. On the other hand, there is no significant effect of the temperature on the selectivity of 1,2-PDO up to 473 K. After 473 K, a slight decrease in the selectivity of 1,2-PDO was observed, which might be due to the easy C–C bond cleavage of the glycerol with acceleration of the reaction rate at high reaction temperatures [62,63]. The apparent activation energies evaluated from the Arrhenius plot were found to be ~58.3 and 26.6 kJ mol^{-1} for the Cu/Mg and Cu/Ce3/Mg catalysts, respectively (Fig. S4 of the Supplementary material). These results indicate that the hydrogenolysis of glycerol over the developed catalysts is kinetically controlled.

The influence of reaction time was examined for the hydrogenolysis of glycerol over the Cu/Ce3/Mg and Cu/Mg catalysts. The achieved results are shown in Fig. 9. The reaction was performed by varying the reaction time at a temperature of 473 K and hydrogen pressure of 60 bar for both catalysts using 20 wt.% aqueous glycerol solution. In the case of Cu/Mg catalyst, by increasing the reaction time from 5 to 20 h, an improvement in the glycerol conversion from 21 to 56% was found. After 20 h, there was no considerable change in the glycerol conversion. On the other hand, the selectivity of 1,2-PDO was gradually decreased with reaction time. These results indicate that the efficiency of the Cu/Mg catalyst toward the product selectivity was decreased, which may be due to the deactivation of the catalyst after 20 h of reaction time.In the case of the Cu/Ce3/Mg sample the glycerol conversion was rapidly increased with increasing reaction time up to 25 h, while no considerable decrease was observed in the 1,2-PDO selectivity. By increasing the reaction time to 35 h the maximum glycerol conversion and selectivity of 1,2-PDO were reached to 88.4 and 87%, respectively. At higher glycerol conversions the reaction rate was found to be quite low, which is due to a decrease in the glycerol concentration or/and a competition for active sites between glycerol and 1,2-PDO.

The effect of hydrogen pressure on the hydrogenolysis of glycerol was investigated by varying the H_2 pressure from 20 to 80 bar using 10 wt.% of the Cu/Ce3/Mg sample (with respect to the initial glycerol weight), 20 wt.% of 50 g of aqueous glycerol solution, 473 K reaction temperature, and 10 h of reaction time. The obtained results are presented in Fig. 10. It was found that the increase of H_2 pressure positively affects on both glycerol conversion and 1,2-PDO selectivity. It was reported that the active hydrogen species on metal sites increase by increasing H_2 pressure, hence enhanced rate of acetol hydrogenation [64,65]. At lower H_2 pressure (20 bar), the glycerol conversion and selectivity of 1,2-PDO are found to be approximately 28.8% and 93%, respectively. Under these reaction conditions the selectivity of acetol was found to be more because lower hydrogen pressure seems to be insufficient for the hydrogenation of acetol to produce desired 1,2-PDO. By increasing

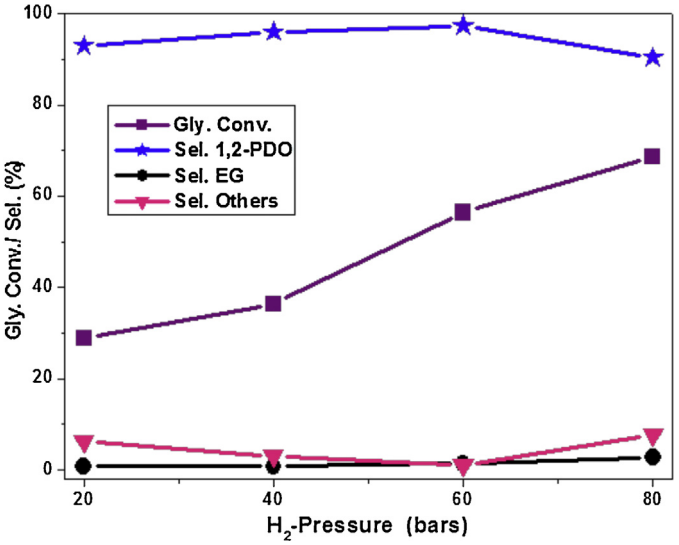

Fig. 10. Effect of H_2 pressure on the glycerol conversion and the selectivity of 1,2-PDO over the Cu/Ce3/Mg catalysts. Reaction conditions: 50 g of 20 wt.% aqueous glycerol solutions, 1 g of reduced catalyst, 10 h of reaction time and 300 rpm of stirring speed with 473 K of reaction temperature.

hydrogen pressure up to 60 bar the glycerol conversion and selectivity of 1,2-PDO were increased. At higher hydrogen pressures, there is no change in the selectivity of ethylene glycol, because copper is responsible for cleavage of C–O bond only, but not for the C–C bond cleavage even in the presence of high H_2 pressure. The achieved glycerol conversions were 28.8, 36.4, 56.4, and 68.7% for the H_2 pressures of 20, 40, 60, and 80 bar, respectively. This observation is probably due to the fact that an easy C–O bond cleavage can be occurred at higher hydrogen pressures [66]. It is therefore concluded that the higher hydrogen pressures favor the hydrogenation of acetol to obtain the 1,2-PDO in the hydrogenolysis of glycerol.

The influence of glycerol concentration on the glycerol hydrogenolysis was examined at the glycerol wt.% of 20, 40, 60, and 80 (Fig. S5 of the Supplementary material). With the increase of glycerol concentration from 20 to 80%, the glycerol conversion and 1,2-PDO selectivity were decreased from 56 to 45% and 97 to 91%, respectively. The decrease of glycerol conversion is expected with the increase of the glycerol concentration because the number of available active sites on the catalyst is constant [7]. Another important fining is that the Cu/Ce3/Mg catalyst maintains high 1,2-PDO selectivity even at high glycerol concentration.

The effect of water on the glycerol hydrogenolysis was studied over the Cu/Ce3/Mg catalyst (Table 3). It was reported that water as a solvent strongly affect the product distribution in the glycerol hydrogenolysis [67]. As shown in Scheme 1, the glycerol hydrogenolysis reaction follows the dehydration–hydrogenation pathway. This reaction was investigated using pure glycerol and 10–50 wt.% aqueous glycerol solution under the standard conditions of 473 K reaction time, 60 bar H_2 pressure and 10 h reaction time. The amount of the catalyst used in each reaction was adapted so as to keep the weight ratio of the catalyst to glycerol remains constant. As stated, the glycerol conversion was slightly decreased with increasing water quantity. In the diluted glycerol solution (20 wt.% of aqueous glycerol), the selectivity of 1,2-PDO is 97.24% whereas in case of the pure glycerol the selectivity is 81.5%. Water retard the C–C bond breakage reaction, hence the selectivity toward ethylene glycol reduces with the increase of its quantity [67]. Therefore, the experimental results indicate that the selective hydrogenolysis of bioglycerol to 1,2-PDO is more pronounced in the presence of water.

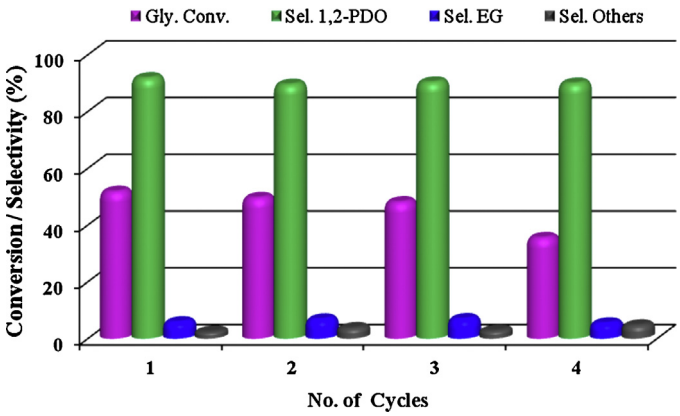

Fig. 11. Reusability study of Cu/Ce3/Mg catalyst for the hydrogenolysis of glycerol. Reaction conditions: 50 g of 20 wt.% aqueous glycerol solutions, 473 K of temperature, 60 bar of H_2 pressure, 1 g of reduced catalyst, 300 rpm of stirring speed, and 10 h of reaction time.

The effect of the catalyst weight on the glycerol hydrogenolysis was also studied (Fig. S6 of the Supplementary material). It was found that the glycerol conversion increases with the increase of the catalyst amount. The obtained glycerol conversion at 5, 10, 15, and 20 wt.% was 24.9, 56.4, 64.1, and 75.3%, respectively. It is well-known that increasing the catalyst weight leads to an increase in the number of available active sites, resulting in improved efficacy of the catalyst. Hence, higher glycerol conversions were found at high catalyst loadings. In contrast, the 1,2-PDO selectivity was decreased from 92 to 89% with increasing the catalyst amount from 5 to 20 wt.%, respectively. This result might be due to the availability of excess reaction active sites (e.g., acidic sites, oxygen vacancies, and metal sites), resulting in further hydrogenation of 1,2- PDO to produce lower alcohols, such as 1-propanol, 2-propanol, and ethanol [21].

3.2. Stability and reusability test

To understand the catalyst stability and reusability, we have studied the efficiency of the Cu/Ce3/Mg catalyst up to 4 cycles for the glycerol hydrogenolysis (Fig. 11). The reusability study was performed at the following conditions: 473 K of reaction temperature, 60 bar of H_2 pressure, 50 g of 20 wt.% aqueous glycerol solution, 1 g of reduced catalyst, stirring speed of 300 rpm, and 10 h of reaction time. After each experiment, the catalyst was separated from the reaction mixture by centrifugation and then, the catalyst was washed with methanol and dried at 393 K for 12 h. Subsequently, the catalyst was subjected to reduction at 573 K for 3 h. The obtained glycerol conversions were 51.8, 49.6, 48.1 and 35.5% over Cu/Ce3/Mg catalyst at 1st, 2nd, 3rd, and 4th cycles, respectively. It is understood that there was no significant variation in the efficacy of the catalyst up to 3rd cycle and then, its efficiency was slightly decreased. It is interesting to note here that the selectivity of 1,2-PDO is almost same for all cycles. These results indicate the significant of present work in the selective hydrogenolysis of glycerol.

We have performed few analysis investigations to understand the factors responsible for the deactivation of the catalyst after the third cycle. The N_2 adsorption–desorption isotherms and pore size distribution profiles of the fresh, reduced, and spent Cu/Ce3/Mg catalysts (3rd cycle) are shown in Fig. 12. As noticed from Fig. 12, all catalysts exhibit Type IV with a H1 hysteresis loop, which indicates typical mesoporous nature of the materials. The achieved specific surface area was ~209, 120 and 51 m^2/g for the fresh, reduced, and spent catalysts, respectively (Table 4). Moreover, the pore volume of fresh, reduced and spent Cu/Ce3/Mg samples were found to be

Table 3
Effect of water as solvent on glycerol hydrogenolysis reaction over Cu/Ce3/Mg catalyst. 1,2-PDO: 1,2-propanediol and EG: ethylene glycol.

Glycerol:water (g)	Catalyst wt. (g)	Glycerol conversion (%)	Product selectivity (%)		
			1,2-PDO	EG	Others
05:45	0.5	39.4	97.5	1.7	0.8
10:40	1.0	56.4	97.4	1.4	1.2
15:35	1.5	61.2	95.2	3.6	1.2
20:30	2.0	66.6	94.8	3.3	1.9
25:25	2.5	70.1	92.3	5.3	2.4
Pure glycerol	5.0	73.7	81.5	12.2	6.3

Reaction conditions: 473 K of temperature, 60 bar of H_2 pressure, 300 rpm of stirring speed and 10 h of reaction time.

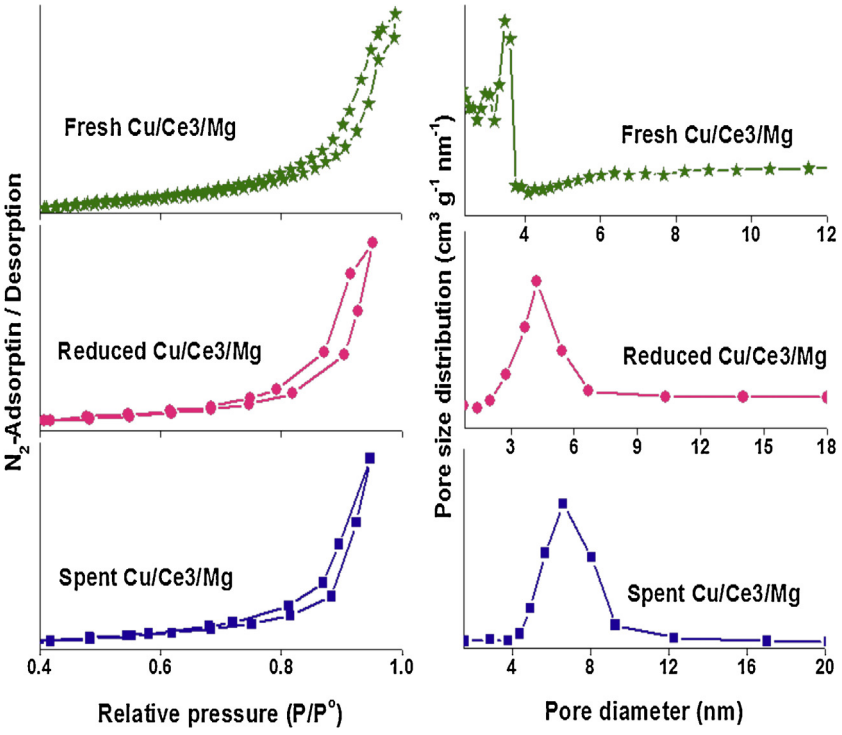

Fig. 12. N_2 adsorption–desorption isotherms and pore size distribution spent, reduced, and fresh Cu/Ce3/Mg catalyst.

Table 4
Physicochemical properties of the fresh, reduced, and spent Cu/Ce3/Mg catalysts.

Property	Fresh Cu/Ce3/Mg	Reduced Cu/Ce3/Mg	Spent Cu/Ce3/Mg
BET surface area	209	120	51
Pore volume	0.569	0.425	0.263
Pore size	10.861	12.020	11.425
I_{Ov}/I_{F2g} value	0.668	0.336	0.009

0.569, 0.425 and 0.263 cm^3/g, respectively. The obtained pore size values of fresh, reduced and spent catalysts were 10.86, 12.02 and 11.42 nm (Table 4), respectively. As observed in fresh Cu/Ce3/Mg sample (Fig. 1), reduced and spent samples also exhibited typical XRD peaks of fluorite cubic structured CeO_2 (Fig. S7 of the Supplementary material). The reduced sample shows two XRD peaks at 43.3 and 50.4°, which can be assigned to metallic copper in agreement with the literature reports [28,68–70]. As well, these two peaks were merged with the MgO peaks, hence the calculation of average crystallite size of the Cu species was not possible for the reduced one. Interestingly, the reduced Cu/Ce3/Mg sample also exhibited CuO peaks along with the metallic Cu peaks [71]. This is due to the fact that the reduced sample is exposed to air before XRD analysis (ex-situ analysis), hence some proportion of the metallic copper can be partially re-oxidized to CuO. But, it could be understood that the metallic Cu species were formed from the reduction of CuO species as evidenced by the H_2-TPR analysis (Fig. 5). Hence, it can be expected that the sample exhibits metallic Cu species after the reduction of the catalyst. Clearly noticed from XRD profile, there are no peaks observed for metallic Cu in the spent Cu/Ce3/Mg sample (Fig. S7 of the Supplementary material). This observation indicates the re-oxidation of metallic Cu species to CuO during the reaction [71]. Fig. 13 shows Raman spectra of the fresh, reduced, and spent Cu/Ce3/Mg catalysts. As can be noted from Fig. 13 and Table 4, the O_v/F_{2g} ratio is significantly decreased after the 3rd cycle. Based on these results, it can be stated that the variation in the physicochemical properties of the Cu/Ce3/Mg catalyst is a key reason for its deactivation in the hydrogenolysis of glycerol after the 3rd cycle. All these characterization studies have been performed in the ex-situ conditions. The characterization of reduced

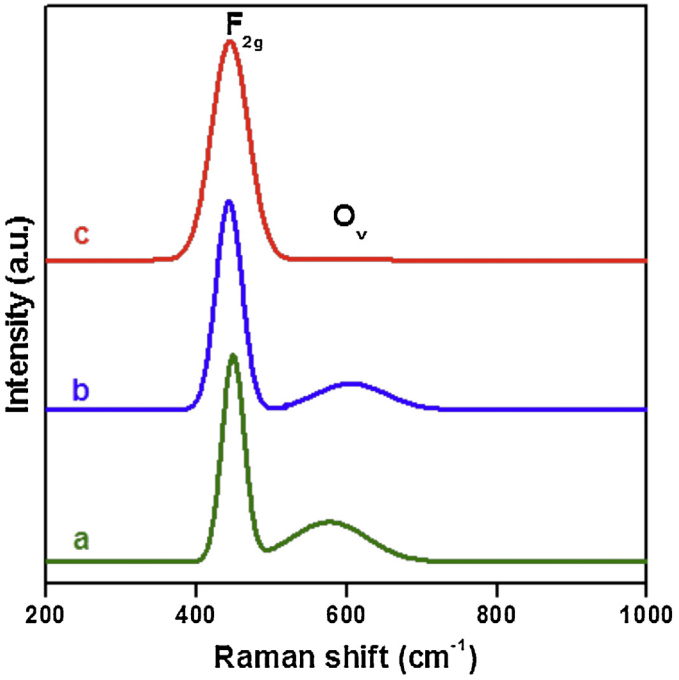

Fig. 13. Visible Raman spectra of (a) fresh, (b) reduced, and (c) spent Cu/Ce3/Mg catalysts.

sample using in-situ conditions is necessary to exactly understand the properties of reduced sample, which is under investigation.

4. Conclusions

In this work, a series of Ce-promoted Cu/Mg and the unpromoted Cu/Mg catalysts were synthesized by an economical coprecipitation method. The catalytic efficiency of the materials was studied for the hydrogenolysis of glycerol to produce 1,2-propanediol. The investigated characterization studies revealed that the addition of Ce to the Cu–Mg sample significantly enhances its structural, acid and redox properties. It was found that the Ce-promoted Cu/Mg catalysts exhibit a higher catalytic performance for the hydrogenolysis of glycerol. Among the Ce-promoted Cu/Mg catalysts, the Cu/Ce3/Mg catalyst showed better catalytic activity due to higher concentration and superior strength of acidic sites, abundant oxygen vacancy defects, and enhanced reducible nature. The achieved activity order of the investigated catalysts is Cu/Mg < Cu/Ce1/Mg < Cu/Ce5/Mg < Cu/Ce3/Mg. The estimated activation energy was found to be ~58.3 and 26.6 kJ mol^{-1} for the Cu/Mg and Cu/Ce3/Mg catalysts, respectively. The catalytic performance of the Cu/Ce3/Mg sample was remained same up to 3 cycles. Afterwards, its efficiency was slightly decreased due to unfavorable properties of the catalyst.

Acknowledgments

BM and BVSR thank the Council of Scientific and Industrial Research (CSIR), New Delhi for senior research fellowships. Financial support for this project was received from Department of Science and Technology, New Delhi, under SERB Scheme (SB/S1/PC-106/2012).

Appendix A. Supplementary data

Supplementary data associated with this article can be found, in the online version, at http://dx.doi.org/10.1016/j.apcatb.2015.07.037

References

[1] L. Xin, Z. Zhang, J. Qi, D.J. Chadderdon, Y. Qiu, K.M. Warsko, W. Li, ChemSusChem 6 (2013) 674–686.
[2] S. Chu, A. Majumdar, Nature 488 (2012) 294–303.
[3] E.L. Kunkes, D.A. Simonetti, R.M. West, J.C. Serrano-Ruiz, C.A. Gartner, J.A. Dumesic, Science 322 (2008) 417–421.
[4] T. Wang, M.W. Nolte, B.H. Shanks, Green Chem. 16 (2014) 548–572.
[5] C.H. Zhou, X. Xia, C.X. Lin, D.S. Tong, J. Beltramini, J. Chem. Soc. Rev. 40 (2011) 5588–5617.
[6] B. Mallesham, P. Sudarsanam, G. Raju, B.M. Reddy, Green Chem. 15 (2013) 478–489.
[7] S. Zhu, X. Gao, Y. Zhu, Y. Zhu, H. Zheng, Y. Li, J. Catal. 303 (2013) 70–79.
[8] M.J. Climent, A. Corma, S. Iborra, Green Chem. 16 (2014) 516–547.
[9] B. Li, J. Wang, Y. Yuan, H. Ariga, S. Takakusagi, K. Asakura, ACS Catal. 1 (2011) 1521–1528.
[10] B. Mallesham, P. Sudarsanam, B.M. Reddy, Catal. Sci. Technol. 4 (2014) 803–813.
[11] S.-I. Fujita, Y. Yamanishi, M. Arai, J. Catal. 297 (2013) 137–141.
[12] M. Gonçalves, V.C. Souza, T.S. Galhardo, M. Mantovani, F.C.A. Figueiredo, D. Mandelli, W.A. Carvalho, Ind. Eng. Chem. Res. 52 (2013) 2832–2839.
[13] S. Demirel, M. Lucas, J. Warna, T. Salmi, D. Murzin, P. Claus, Top. Catal. 44 (2007) 299–305.
[14] P. Sudarsanam, B. Mallesham, A.N. Prasad, P.S. Reddy, B.M. Reddy, Fuel Process. Technol. 106 (2013) 539–545.
[15] B. Katryniok, S. Paul, M. Capron, C. Lancelot, V.B. Baca, P. Reye, F. Dumeignil, Green Chem. 12 (2010) 1625–1922.
[16] B. Mallesham, P. Sudarsanam, B.M. Reddy, Ind. Eng. Chem. Res. 53 (2014) 18775–18785.
[17] E. D'Hondt, S. Van de Vyver, B.F. Sels, P.A. Jacobs, Chem. Commun. (2008) 6011–6012.
[18] G.D. Yadav, P.A. Chandan, D.P. Tekale, Ind. Eng. Chem. Res. 51 (2012) 1549–1562.
[19] J. Hu, Y. Fan, Y. Pei, M. Qiao, K. Fan, X. Zhang, B. Zong, ACS Catal. 3 (2013) 2280–2287.
[20] I. Gandarias, P.L. Arias, J. Requies, M.B. Guemez, J.L.G. Fierro, Appl. Catal. B: Environ. 97 (2010) 248–256.
[21] T. Miyazawa, Y. Kusunoki, K. Kunimori, K. Tomishige, J. Catal. 240 (2006) 213–221.
[22] E.P. Maris, W.C. Ketchie, M. Murayama, R.J. Davis, J. Catal. 251 (2007) 281–294.
[23] E.P. Maris, R.J. Davis, J. Catal. 249 (2007) 328–337.
[24] S. Zhu, X. Gao, Y. Zhu, Y. Zhu, X. Xiang, C. Hu, Y. Li, Appl. Catal. B: Environ. 140–141 (2013) 60–67.
[25] T.A. Werpy, J. John, G. Frye, A.H. Zacher, D.J. Miller, US Patents 6841 (2005) 085.
[26] P. Alvise, T. Pietro, Ind. Eng. Chem. Res. 44 (2005) 8535–8537.
[27] Z.W. Huang, F. Cui, H.X. Kang, J. Chen, X.Z. Zhang, C.G. Xia, Chem. Mater. 20 (2008) 5090–5099.
[28] Z. Huang, H. Liua, F. Cui, J. Zuo, J. Chen, C. Xia, Catal. Today 234 (2014) 223–232.
[29] A.Y. Yin, X.Y. Guo, W.Y. Dai, K.N. Fan, Green Chem. 11 (2011) 1514–1516.
[30] A. Wolosiak-Hnat, E. Milchert, B. Grzmil, Chem. Eng. Technol. 36 (2013) 411–418.
[31] D. Coll, F. Delbecq, Y. Aray, P. Sautet, Phys. Chem. Chem. Phys. 13 (2011) 1448–1456.
[32] Z. Yuan, J. Wang, L. Wang, W. Xie, P. Chen, Z. Hou, X. Zheng, Bioresour. Technol. 101 (2011) 7088–7092.
[33] Z. Yuan, L. Wang, J. Wang, S. Xia, P. Chen, Z. Hou, X. Zheng, Appl. Catal. B: Environ. 101 (2011) 431–440.
[34] I. Jiménez-Moralesa, F. Vila, R. Mariscal, A. Jiménez-Lópeza, Appl. Catal. B: Environ. 117–118 (2012) 253–259.
[35] W. Yu, J. Zhao, H. Ma, H. Miao, Q. Song, J. Xu, Appl. Catal. A 83 (2010) 73–78.
[36] J.-L. Liu, L.-J. Zhu, Y. Pei, J.-H. Zhuang, H. Li, H.-X. Li, M.-H. Qiao, K.-N. Fan, Appl. Catal. A: Gen. 353 (2009) 282–287.
[37] J. Chen, J. Zhu, Y. Zhan, X. Lin, G. Cai, K. Wei, Q. Zheng, Appl. Cata. A: Gen. 363 (2009) 208–215.
[38] S. Wang, H. Liu, Catal. Lett. 117 (2007) 62–67.
[39] L. Katta, P. Sudarsanam, B. Mallesham, B.M. Reddy, Catal. Sci. Technol. 2 (2012) 995–1004.
[40] B.M. Reddy, G. Thrimurthulu, L. Katta, Y. Yamada, S.-E. Park, J. Phys. Chem. C 113 (2009) 15882–15890.
[41] B.M. Reddy, L. Katta, G. Thrimurthulu, Chem. Mater. 22 (2010) 467–475.
[42] P. Sudarsanam, P.R. Selvakannan, S.K. Soni, S.K. Bhargava, B.M. Reddy, RSC Adv. 4 (2014) 43460–43469.
[43] G. Diaz, R. Perez-Hernandez, A. Gomez-Cortes, M. Benaissa, R. Mariscal, J.L.G. Fierro, J. Catal. 187 (1999) 1–14.
[44] A. Auroux, A. Gervasini, C. Guimon, J. Phys. Chem. B 103 (1999) 7195–7205.

[45] C.-C. Li, Y.-W. Chen, R.-J. Lin, C.-C. Chang, K.-H. Chen, H.-P. Lin, L.-C. Chen, Chem. Commun. 47 (2011) 9414–9416.
[46] J. Zhou, L. Guo, X. Guo, J. Mao, S. Zhang, Green Chem. 12 (2010) 1835–1843.
[47] R.T. Figueiredo, H.M.C. Andrade, J.L.G. Fierro, J. Mol. Catal. A: Chem. 318 (2010) 15–20.
[48] P. Sudarsanam, B. Mallesham, P.S. Reddy, D. Großmann, W. Grünert, B.M. Reddy, Appl. Catal. B: Environ. 144 (2014) 900–908.
[49] L. Katta, P. Sudarsanam, G. Thrimurthulu, B.M. Reddy, Appl. Catal. B: Environ. 101 (2010) 101–108.
[50] V. Fournier, P. Marcus, I. Olefjord, Surf. Interface Anal. 34 (2002) 494–497.
[51] K.N. Rao, P. Venkataswamy, B.M. Reddy, Ind. Eng. Chem. Res. 50 (2011) 1196–11960.
[52] X.M. Guo, D.S. Mao, G.Z. Lu, S. Wang, G.S. Wu, J. Catal. 271 (2010) 178–185.
[53] P. Gao, F. Li, H. Zhan, N. Zhao, F. Xiao, W. Wei, L. Zhong, H. Wang, Y. Sun, J. Catal. 298 (2013) 51–60.
[54] L. Liu, Z. Yao, B. Liu, L. Dong, J. Catal. 275 (2010) 45–60.
[55] F. Mauriello, H. Ariga, M.G. Musolino, R. Pietropaolo, S. Takakusagi, K. Asakur, Appl. Catal. B: Environ. 166–167 (2015) 121–131.
[56] Y. Shinmi, S. Koso, T. Kubota, Y. Nakagawa, K. Tomishige, Appl. Catal. B: Environ. 94 (2010) 318–326.
[57] J. Ge, Z. Zeng, F. Liao, W. Zheng, X. Hong, S.C.E. Tsang, Green Chem. 15 (2013) 2064–2069.
[58] A. Martin, U. Armbruster, I. Gandarias, P.L. Arias, Eur. J. Lipid Sci. Technol. 115 (2013) 9–27.
[59] M.G. Musolino, L.A. Scarpino, F. Mauriello, R. Pietropaolo, ChemSusChem 4 (2011) 1143–1150.
[60] E.S. Vasiliadou, E. Heracleous, I.A. Vasalos, A.A. Lemonidou, Appl. Catal. B: Environ. 92 (2009) 90–99.
[61] M.A. Dasari, P.-P. Kiatsimkul, W.R. Sutterlin, G.J. Suppes, Appl. Catal. A: Gen. 281 (2005) 225–231.
[62] A. Bienholz, F. Schwab, P. Claus, Green Chem. 12 (2010) 290–295.
[63] L. Huang, Y.-L. Zhu, H.-Y. Zheng, Y.-W. Li, Z.-Y. Zeng, J. Chem. Technol. Biotechnol. 83 (2008) 1670–1675.
[64] I. Jiménez-Morales, F. Vila, R. Mariscal, A. Jiménez-López, Appl. Catal. B: Environ. 117–118 (2012) 253–259.
[65] E.S. Vasiliadou, T.M. Eggenhuisen, P. Munnik, P.E. de Jongh, K.P. de Jong, A.A. Lemonidou, Appl. Catal. B: Environ. 145 (2014) 108–119.
[66] L.C. Meher, R. Gopinath, S.N. Naik, A.K. Dalai, Ind. Eng. Chem. Res. 48 (2009) 1840–1846.
[67] E.S. Vasiliadou, A.A. Lemonidou, Org. Process Res. Dev. 15 (2011) 925–931.
[68] Z. Huang, J. Chen, Y. Jia, H. Liu, C. Xia, H. Liu, Appl. Catal. B: Environ. 147 (2014) 377–386.
[69] Z. Huanga, F. Cuia, J. Xue, J. Zuo, J. Chen, C. Xia, Catal. Today 183 (2012) 42–51.
[70] H. Liu, Z. Huang, C. Xia, Y. Jia, J. Chen, H. Liu, ChemCatChem 6 (2014) 2918–2928.
[71] A. Bienholz, R. Blume, A. Knop-Gericke, F. Girgsdies, M. Behrens, P. Claus, J. Phys. Chem. C 115 (2011) 999–1005.